이학석사학위논문

탄키라아제 억제를 통한 골관절염 연골의 내재된 회복 능력 활성화

Tankyrase inhibition stimulates innate repair capacity in osteoarthritic cartilage

2018년 2월

서울대학교 대학원

생명과학부

김 수 경

탄키라아제 억제를 통한 골관절염 연골의 내재된 회복 능력 활성화

Tankyrase inhibition stimulates innate repair capacity in osteoarthritic cartilage

지도교수 김 진 홍

이 논문을 이학석사 학위논문으로 제출함

2017년 12월

서울대학교 대학원
생명과학부
김 수 경

김수경의 석사 학위논문을 인준함
2017년 12월

위 원 장 ____김 재 범____ (인)

부위원장 ____김 진 홍____ (인)

위   원 ____최 희 정____ (인)

Abstract

Tankyrase inhibition stimulates innate repair capacity in osteoarthritic cartilage

Sukyeong Kim

School of Biological Sciences

The Graduate School

Seoul National University

Osteoarthritis (OA) is a prevalent degenerative disease, which involves progressive and irreversible destruction of articular cartilage. Despite efforts to regenerate cartilage in osteoarthritic joints, it has been a difficult task as adult cartilage exhibits marginal self-repair capacity. I conducted systems-level factor analysis on mouse reference populations and identified tankyrase as a regulator of the cartilage anabolism axis. Tankyrase inhibition increases the collective expression of cartilage-specific matrix genes in mouse chondrocytes. Moreover, tankyrase inhibition stimulates chondrogenic differentiation of mesenchymal stem cells from mouse limb-bud and human bone marrow. In osteochondral defect model of rats, stem-cell transplantation coupled with tankyrase knockdown results in superior

regeneration of cartilage lesions. Mechanistically, the pro-regenerative features of tankyrase inhibition are mainly triggered by regulating SOX9 transcriptional activity. I found that tankyrase binds to and poly(ADP-ribosyl)ates (PARylates) SOX9. Furthermore, in surgically induced OA mouse model, treatment of hydrogel-based tankyrase inhibitor ameliorates OA progression. These results suggest that tankyrase inhibition in treating OA cartilage may be a potential strategy for functional repair of articular cartilage.

CONTENTS

Reprinted from the manuscript prepared for publication

LIST OF FIGURES

LIST OF SUPPLEMENTARY TABLES

INTRODUCTION

Osteoarthritis (OA) is one of the most prevalent degenerative diseases involving progressive degeneration of articular cartilage.

Osteoarthritis (OA) is one of the most prevalent d e g e n e r a t i v e diseases and one of the leading causes of chronic disability in elderly populations. Its prevalence is increasing worldwide, imposing a tremendous medical and socioeconomic burden. OA is primarily characterized by the loss of proteoglycan contents and collagen degradation in cartilage matrix. The degeneration of cartilage matrix during OA development eventually causes failure in load-bearing functions of articular cartilage, further linking to subchondral bone damage and joint pain (Wieland et al., 2005).

Disease-modifying OA therapy essentially aimed prolonged and functional repair of articular cartilage.

Cartilage repair is steered by chondrogenic differentiation of resident progenitor cells and ECM anabolism by the differentiated chondrocytes, but these abilities generally decline with aging and the disease progression, leaving only a marginal repair capacity in osteoarthritic joints (Johnson et al., 2012; Heinemeier et al., 2016). To compensate for the lack of innate repairing abilities, stem-cell based therapies utilizing enrichment of mesenchymal stem cell population by marrow stimulation (Sakata et al., 2013) or direct transplantation (Diekman and Guilak, 2013) into damaged region has been rigorously attempted. However, cells differentiated from these progenitors tend to rapidly lose characteristic features of chondrocytes with concomitant cessation of cartilage-specific matrix molecule synthesis (Sakata et al., 2013; Diekman and Guilar, 2013).

Recent studies have focused on elimination of catabolic factors that develop

cartilage destruction.

There are many causes that progress OA, for example, joint instability and injury, and aging. These activate catabolic biochemical pathways in chondrocytes including matrix degrading enzymes, matrix metalloproteinases (MMPs) and aggrecanases (ADAMTSs). This results in degradation of cartilage matrix and deterioration in OA symptoms. Thus, inhibiting these catabolic factors serve as an attractive therapeutic approach that delays erosion of the cartilage matrix and further OA advancement.

Particularly, recent trends in research as a new therapeutic strategy for treating degenerative cartilage are removing cells aged in cartilage and bone tissue and expressing a matrix degrading enzyme protein and inflammation-related proteins, that can accelerate the progression of degenerative arthritis (Farr et al., 2017; Jeon et al., 2017). In addition, when traumatic arthritis is induced, chondrocytes in the superficial zone of the joints' cartilage express catabolic mediators and cause cartilage damages. Inducing superficial chondrocyte death reduces the progression of murine posttraumatic osteoarthritis (Zhang et al., 2016).

Delaying cartilage damage through inhibition of catabolic factors is insufficient to obtain the regenerative effect in cartilage tissue.

A therapeutic strategy by finding factors and cells that regulate cartilage degeneration and eliminating them is merely possible to delay in the progression of cartilage degeneration. There is a limit to regenerating the cartilage matrix in which destruction has progressed.

Moreover, because degenerative arthritis is more common in elderly people and cartilage tissue of aged mammals spontaneously undergoes almost no turnover, side-effects are expected when applying a method of removing cartilage cells as a treatment for patients with degenerative arthritis.

Stimulating the innate repair capacity in articular cartilage will be possible through activation of cartilage anabolic genes.

The current paradigm is that articular cartilage possesses only a marginal capacity for self-repair, partly because this avascular tissue has limited access to nutrients and oxygen. Furthermore, this regenerative capacity appears to further decline with age and post-traumatic events, rendering OA an irreversible degenerative disease of the connective tissues. I undertook this study to investigate whether it is feasible to stimulate the innate repair capacity of articular cartilage and possibly reverse the disease progression of OA.

Here, I demonstrate that tankyrase inhibition serves as a potential therapeutic strategy, enabling reconstruction of the cartilage matrix and reversion of OA-associated phenotypes, at both the molecular and organismal levels.

MATERIALS AND METHODS

In silico **analysis of multi-tissue transcriptomes of the BXD mouse population.**

Cartilage (GN208) (Suwanwela et al., 2011), bonefemur(GN411) (Farber et al., 2009), kidney(GN118), lung(GN160) (Alberts et al., 2011), andbrain(GN123) (Saba et al., 2006) data sets were obtained from GeneNetwork (www.genenetwork.org). Probes in the data sets were reannotated using the illuminaMousev1.db 1.26.0, lluminaMousev1p1.db 1.26.0, or mouse4302.db 3.2.3 R packages. For the cartilage and bone femur data sets, a probe having non-overlapping SNPs, 'Perfect' quality, and the highest expression was used for each transcript. For the other data sets, the probe with the highest expression was used for each transcript. Data values were clustered using the hierarchical clustering algorithm (complete linkage and uncentered correlation distance) in Cluster 3.0 (http://bonsai.hgc.jp/~mdehoon/software/cluster/software.htm), and correlation heatmaps were drawn with Gitools 2.3.1 (Perez-Llamas and Lopez-Bigas, 2011). Factor analysis was performed using IBM SPSS Statistics 24 (http://www.ibm.com/analytics/us/en/technology/spss/). Principal component analysis was used to extract two factors, and factor scores were calculated using a regression method.

Animals.

All animal studies were conducted with the approval of the Seoul National University Institutional Animal Care and Use Committee (IACUC). I conformed to the ARRIVE guidelines (https://www.nc3rs. org.uk/arrive-guidelines) for reporting animal experiments (Kilkenny et al., 2010).

Primary culture of mouse articular chondrocytes.

For the primary culture of mouse articular chondrocytes, cells were isolated from femoral condyles and tibial plateaus of 4–5-day-old ICR mice, as described previously (Gosset et al., 2008). Chondrocytes were maintained in DMEM supplemented with 10% fetal bovine serum (FBS), 100 units/ml penicillin, and 100 μg/ml streptomycin, and cells were treated as indicated in each experiment. Transfection was performed with METAFECTENE PRO (Biontex) according to the manufacturer's protocol. Small interfering RNAs (siRNAs) used for RNA interference (RNAi) in mouse articular chondrocytes are listed in **Table 1**. All siRNAs, including negative control siRNA, were purchased from Bioneer.

Tankyrase, PARP1/2, or β-catenin responsive transcription inhibitors.

XAV939 (X3004), IWR-1 (I0161), JW55 (SML0630), and WIKI4 (SML0760) were obtained from Sigma-Aldrich. G007-LK (B5830) was purchased from Apexbio, G244-LM (1563007-08-8) was from AOBIOUS, MN-64 (HY19351) from MedChem Express, and AZ6102 (S7767) from SelleckChem, and TC-E 5001 (5049) from Tocris. Tankyrase inhibitors were classified into three different classes depending on their mode of action (Lehtio and Krauss, 2013; Haikarainen et al., 2014). ABT-888 (11505) was purchased from Cayman.

RT-PCR and qPCR.

Total RNAs were extracted using TRI reagent (Molecular Research Center, Inc.). RNAs were reverse transcribed using EasyScript Reverse Transcriptase (Transgen Biotech). Then, cDNA was amplified by PCR or qPCR with the primers listed in **Table 2**. qPCR was performed with SYBR TOPreal qPCR 2× preMIX (Enzynomics) to determine transcript abundance. Transcript quantity was calculated using the $\Delta\Delta C_t$ method, and *Hprt* or

HPRT1 levels were used as housekeeping controls. The $\log_2$ (fold change) values of cartilage matrix genes in siRNA-treated mouse articular chondrocytes were clustered using the hierarchical clustering algorithm (average linkage and centered correlation distance) in the factoextra 1.0.4 R package. PCA was conducted using the same R package.

Antibodies.

Anti-FLAG tag antibody (3165) was purchased from Sigma-Aldrich. Antibodies against GFP (sc-9996), Sox-9 (sc-20095), Tankyrase-1/2 (sc-8337), Actin (sc-1615), Ubiquitin (sc-8017), normal mouse IgG (sc-2025), and normal rabbit IgG (sc-2027) were purchased from Santa Cruz Biotechnology. The antibody against Sox-9 from Santa Cruz was used only in **Figure 7e**. Antibodies against aggrecan (AB1031) and type II collagen (MAB8887) were purchased from Millipore, and antibodies against Myc tag (2276) and Sox9 (82630) were purchased from Cell Signaling Technology. Prior to detection of aggrecan, samples were treated with chondroitinase ABC (C3667) from Sigma-Aldrich. Antibodies against HA tag (ab911) were purchased from Abcam. All primary antibodies were used according to the manufacturer's protocol.

Whole-cell lysate preparation.

Whole-cell lysates were prepared in RIPA buffer (150 mM NaCl, 1% NP-40, 50 mM Tris, pH 8.0, 0.5% sodium deoxycholate, 0.1% SDS) supplemented with a protease inhibitor cocktail (Sigma-Aldrich). The lysates were quantified using a BCA assay and analyzed by SDS-PAGE.

Mouse limb-bud micromass culture.

For the micromass culture of mesenchymal cells, limb-bud cells were isolated from E11.5 ICR mouse embryos. 2.0×10^7 cells/ml were suspended

in DMEM supplemented with 10% FBS, 100 units/ml penicillin, and 100 μg/ml streptomycin, and 15-μl drops were spotted on culture dishes. After 24 h, cells were treated as indicated for 3 days and subjected to Alcian Blue staining.

Tri-lineage differentiation of human mesenchymal stem cells.

hMSCs were purchased from Lonza and Thermo Scientific. hMSCs were cultured in α-MEM supplemented with 20% FBS, 100 units/ml penicillin, 100 μg/ml streptomycin, and 250 ng/ml amphotericin B. To induce osteogenesis or adipogenesis, 1.0×10^5 hMSCs were cultured in 12-well plates with osteogenic medium with or without indicated drugs for 14 days or adipogenesis medium with or without indicated drugs for 18 days, respectively. Osteogenic medium consisted of α-MEM supplemented with 10% FBS, 100 units/ml penicillin, 100 μg/ml streptomycin, 250 ng/ml amphotericin B, 50 μM L-ascorbic acid, 0.1 μM dexamethasone, and 10 mM β-glycerophosphate. Adipogenic medium consisted of α-MEM supplemented with 10% FBS, 100 units/ml penicillin, 100 μg/ml streptomycin, 250 ng/ml amphotericin B, 0.5 mM 3-isobutyl-1-methylxanthine, 1 μM dexamethasone, and 200 μM indomethacin. To analyze differentiation, Oil Red O or Alizarin Red S staining was used. To induce chondrogenesis, 2.5×10^5 hMSCs were centrifuged to form a pellet in α-MEM supplemented with 20% FBS, 100 units/ml penicillin, 100 μg/ml streptomycin, and 250 ng/ml amphotericin B. After 3 days, the medium was changed to chondrogenic medium consisting of DMEM/F-12 supplemented with 100 units/ml penicillin, 100 μg/ml streptomycin, 250 ng/ml amphotericin B, 1.25 mg/ml BSA, 1% Insulin-Transferrin-Selenium, 1 mM Sodium pyruvate, 50 μM L-aspartic acid, 50 μM L-proline, 100 nM dexamethasone, and 10 ng/ml of TGF-β1 with or without indicated drugs. On day 21 (for drug treatment) or day 28 (for

siRNA treatment), cells were harvested and subjected to Alcian Blue/Fast Red staining.

Plasmids.

Human *SOX9* cDNA (hMU008919) was purchased from Korea Human Gene Bank and subcloned into a pcDNA3-HA plasmid. To generate mutant constructs, PCR-mediated mutagenesis was conducted. The GFP-tagged human TNKS1 plasmid was a gift from Dr. Chang-Woo Lee, and the Myc-tagged human TNKS2 plasmid was a gift from Dr. Junjie Chen. The SOX9 reporter construct was a gift from Dr. Veronique Lefebvre. Human *TNKS2* cDNA was subcloned into a pEGFP-C1 plasmid to construct a GFP-tagged human TNKS2 plasmid. A control shRNA sequence was inserted into the pLKO.1 puro and pLKO.1 hygro plasmids. Human *TNKS1* and *TNKS2* shRNA sequences were inserted into the pLKO.1 puro and pLKO.1 hygro plasmids, respectively. The shRNA sequences targeting human *TNKS1* or *TNKS2* were as described previously (Huang et al., 2009). Mouse *Tnks1* and *Tnks2* shRNA sequences were inserted into the pLKO.1 puro and pLKO.1 hygro plasmids, respectively. The shRNA sequence targeting mouse *Tnks1* was as described previously (Levaot et al., 2011). The primers used to generate the above plasmids are listed in **Tables 3**,**4** and **5**.

Generation of control shRNA or *TNKS1/2* shRNA–infected human mesenchymal stem cells.

psPAX2 and pMD2.G were transfected to HEK293T. After 3 days, cell supernatants were harvested and filtered through a 0.45-μm filter. hMSCs were treated with 8 μg/ml polybrene and infected with the indicated lentiviruses. Twenty-four hours after infection, hMSCs were selected with 5 μg/ml puromycin and 200 μg/ml hygromycin for 4 days.

Preparation of hydrogels and *in vivo* confirmation of controlled release of embedded molecules.

6-O-Palmitoyl-l-ascorbic acid (76183) was purchased from Sigma-Aldrich. Hydrogels were prepared with 6-O-Palmitoyl-l-ascorbic acid as described previously (Zhang et al., 2015). DiD percholate (5702) purchased from Tocris was loaded into the hydrogels and used for imaging of controlled release in mouse knee joints. PBS-suspended hydrogel (10 μl, PBS:hydrogel = 1:1) containing 50 pmol DiD was administered intra-articularly, and at 1–9 days post-injection, light-emitting diode (LED) and fluorescence images of knee joints were obtained. LuminoGraph II (Atto) was used to acquire the images.

Experimental OA in mice.

Eight-week-old male ICR mice were used for experimental OA. Experimental OA was induced by DMM surgery on the right hindlimb, and sham surgery was conducted on the left hindlimb as a control (Glasson et al., 2007). 10 μl of PBS-suspended hydrogel (PBS:hydrogel = 1:1) containing vehicle or 10 nmol drugs was administered intra-articularly.

Rat osteochondral defect model.

Twelve-week-old male Sprague Dawley rats were used as the osteochondral defect model. To expose the articular cartilage in the knee joints, a medial parapatellar incision was made and the patella was slightly displaced toward the medial condyle. A full-thickness cartilage defect (3 mm × 1 mm × 1 mm) was created using a 1-mm-diameter spherical drill at the surface of the femoral patellar groove. At the same time, hMSCs were suspended in 10 μl of fibrin glue (TISSEEL) by tapping, and implanted on the defect. To avoid immune rejection, cyclosporine A (C988900) from

Toronto Research Chemicals was injected intra-peritoneally every day. At 8 weeks, rats were sacrificed for histological analyses.

Histology and immunohistochemistry.

Mouse or rat knee joint samples were fixed with 4% paraformaldehyde overnight at 4°C, decalcified in 0.5 M EDTA, pH 7.4, for 2–4 weeks at 4°C, and embedded in paraffin. Paraffin blocks were sectioned at a thickness of 6 μm. For Safranin O staining, Alcian Blue/Fast Red staining, or immunostaining, sections were deparaffinized in xylene and hydrated using a graded ethanol series. To assess cartilage destruction, Safranin O stained samples were graded based on the Osteoarthritis Research Society International (OARSI) (Glasson et al., 2010) by three blinded observers. Cartilage regeneration was scored according to the International Cartilage Repair Society (ICRS) scoring system (van den Borne et al., 2003; Mainil-Varlet et al., 2003) by three blinded observers.

Immunoprecipitation.

Cells were treated with 10 μM of MG-132 (A2585) from ApexBio for 6 h before lysis, except for those shown in **Figure 8a** and **9c,d.** Cell lysates were prepared using EBC200 buffer (50 mM Tris-HCl, pH 7.4, 150 mM NaCl, 0.5% NP-40 and 1 mM EDTA) supplemented with the protease inhibitor cocktail. To detect PARylated proteins, 5 μM of ADP-HPD (118415) from Calbiochem was added to the lysis buffer. Cell lysates were used for pulldown with the indicated antibodies and protein A/G-Sepharose beads (GE Healthcare). The mixture was incubated for overnight at 4°C and washed five times with EBC200 buffer. The bound proteins were subjected to SDS-PAGE or LC-MS/MS analysis.

Endogenous TNKS1/2 pulldown and mass spectrometry.

Primary mouse articular chondrocytes were grown for 4 days followed by 6 h of treatment with 10 μM MG132 (Apexbio, A2585). Cells were lysed, and lysates were incubated with normal rabbit IgG or endogenous TNKS1/2. The bound proteins were eluted with 8 M urea in 50 mM NH_4HCO_3 buffer, pH 8.2 for 1 h at 37°C, and in-solution digestion was performed as described previously (Kim et al., 2013). Peptide sequencing was carried out by LC-MS/MS on a Thermo Ultimate 3000 RSLCnano high-pressure liquid chromatography system coupled to a Thermo Q-Exactive Hybrid Quadrupole-Orbitrap mass spectrometer. LC-MS/MS raw data were converted into .mzML files using ProteoWizard MSConvert 3.0.8789 (Chambers et al., 2012), and the MS-GF+ algorithm (Kim and Pevzner, 2014) with a parameter file consisting of no enzyme criteria and static cysteine modification (+57.022 Da) was used for comparison of all MS/MS spectra against the mouse Uniprot database (release 08-Jun-2016). The final peptide identifications had < 1% false discovery rate (FDR) *q,* at the unique peptide level. Only fully tryptic and semitryptic peptides were considered. For each biological replicate, proteins that were detected only once and proteins that were coimmunoprecipitated with normal rabbit IgG were not considered. For proteins detected in more than one biological replicate, the Venn diagram was drawn with eulerAPE v3 (Micallef and Rodgers, 2014).

***In silico* prediction of Tankyrase substrate proteins.**

The 8 × 20 position-specific scoring matrix (PSSM) generated in Guettler et al.[19] was used to calculate a TTS for each octapeptide in the proteins identified by LC-MS/MS.

$$
TTS = \frac{\sum_{pos.=0}^{8} PSSM_{pos.}}{\max\left(\sum_{pos.=0}^{8} PSSM_{pos.}\right)}
$$

Only those proteins having at least one octapeptide with a TTS of $\geq$ 0.385 were considered. This cutoff is the TTS of the TNKS-binding motifs of mouse AXIN1 and AXIN2. AXIN1 and AXIN2, known tankyrase substrates (Huang et al., 2009), have the lowest maximum TTS among the known tankyrase substrates, due to the suboptimal amino acids at the 4th and 5th positions (Guettler et al., 2011). For further screening, the *chondrogenesis* category in IPA (release Sep-2016) (https://www.qiagenbioinformatics.com/products/ingenuity-pathway-analysis/) was used. The mouse proteins in the IPA *chondrogenesis* category are listed in **Table 6**. For the candidate proteins, were calculated for the octapeptides with a TTS of $\geq$ 0.385. The heatmap of TTS and IUPred disorder scores for candidate proteins was drawn with Gitools 2.3.1 (Perez-Llamas and Lopez-Bigas, 2011).

Cell line culture.

HEK293 and HEK293T were cultured in DMEM containing 10% FBS, 100 units/ml penicillin, and 100 μg/ml streptomycin. Transfection was performed with METAFECTENE PRO or PEI transfection reagent (Sigma-Aldrich) according to the manufacturer's protocol. The siRNAs used in HEK293T are listed in **Table 1**. The siRNA sequences targeting *TNKS1* or *TNKS2* were described previously (Huang et al., 2009).

Sequence alignment of TBD1 and TBD2 of SOX9 among vertebrates.

For the sequence alignment of TBD1 and TBD2 of SOX9 among vertebrates, NP_000337.1 (*Homo sapiens* SOX9), NP_035578.3 (*Mus musculus* SOX9), NP_989612.1 (*Gallus gallus* SOX9), NP_001016853.1 (*Xenopus tropicalis* SOX9), and NP_571718.1 (*Danio rerio* SOX9) were used.

Structural modeling of protein-peptide interactions.

GalaxyPepDock (Lee et al., 2015) was used for modeling of the ARC4 domain of human TNKS2 in complex with the TBD1 or TBD2 peptide of human SOX9. The structures of ARC4:3BP2 (PDB ID: 3TWR) and ARC4:MCL1 (PDB ID: 3TWU) were obtained from Guettler et al (Guettler et al., 2011). The ARC4 domain of human TNKS2 (PDB ID: 3TWU_A) and MCL1 peptide (PDB ID: 3TWU_B) were used as templates. The MCL1 peptide was substituted by the TBD1 (255–266 aa) or TBD2 (269–280 aa) peptide of human SOX9 and docked into a complex. The best predicted model for each of ARC4:SOX9 TBD1 and ARC4:SOX9 TBD2 was selected. The model structures were superimposed with ARC4:3BP2 and ARC4:MCL1 and visualized using the BIOVIA Discovery Studio Visualizer 4.0 (http://accelrys.com/products/collaborative-science/biovia-discovery-studio/visualization.html).

Reporter gene assay.

A firefly luciferase reporter plasmid with SOX9-dependent *Col2a1* enhancer elements (Murakami et al., 2000) was used to quantify the transcriptional activity of SOX9. Primary mouse articular chondrocytes or HEK293T cells were transfected with both a reporter plasmid and a constitutive *Renilla* luciferase plasmid. Cells were also treated with siRNAs or drugs as indicated. *Renilla* and firefly luciferase activity were sequentially measured using a Dual Luciferase Assay Kit (Promega). *Renilla* luciferase was used as a control.

Statistical Analysis.

All experiments were carried out independently at least three times. All images are representative of at least three independent trials. For parametric tests, two-tailed Student's *t* test or one-way analysis of variance (ANOVA) followed by Fisher's least significant difference *post-hoc* test were used. For

nonparametric tests, the Mann-Whitney test was used. All statistical analysis was performed using IBM SPSS Statistics 24. A *P*-value < 0.05 was considered statistically significant.

Genes	Strand	siRNA sequences	Species
Tnks1 #1	S	5'-CACAGAGUCACACUGACUAdTdT-3'	Mouse
	AS	5'-UAGUCAGUGUGACUCUGUGdTdT-3'	
Tnks1 #2	S	5'-GUCUGUCGUUGAGUACCUUdTdT-3'	Mouse
	AS	5'-AAGGUACACAACGACAGACdTdT-3'	
Tnks1 #3	S	5'-ACAUAGCAGCGUUACUGAUdTdT-3'	Mouse
	AS	5'-AUCAGUAACGCUGCUAUGUdTdT-3'	
Tnks2 #1	S	5'-CAGUGUAGUUUUGAGUCUAdTdT-3'	Mouse
	AS	5'-UAGACUCAAAACUACACUGdTdT-3'	
Tnks2 #2	S	5'-CUGUUCUGACUGGUGACUAdTdT-3'	Mouse
	AS	5'-UAGUCACCAGUCAGAACAGdTdT-3'	
Tnks2 #3	S	5'-GUGUCUACUUGUAUCACAUdTdT-3'	Mouse
	AS	5'-AUGUGAUACAAGUAGACACdTdT-3'	
TNKS1	S	5'-GCAUGGAGCUUGUGUUAAUUU-3'	Human
	AS	5'-AUUAACACAAGCUCCAUGCUU-3'	
TNKS2	S	5'-GGAAAGACGUAGUUGAAUAUU-3'	Human
	AS	5'-UAUUCAACUACGUCUUUCCUU-3'	

Supplementary Table 1. List of siRNAs.

Genes	Strand	Primer sequences	Species
Hprt	S	5'-AGTCCCAGCGTCGTGATTAG-3'	Mouse
	AS	5'-GTATCCAACACTTCGAGAGGTC-3'	
Tnks1	S	5'-GAAGGAAGGAGAAGTTGCGG-3'	Mouse
	AS	5'-AATGAAAGGAGAACCGTGGAAC-3'	
Tnks2	S	5'-CGGCGTCTTCAACAGATACA-3'	Mouse
	AS	5'-AGCCATCAACCATACCTTCAG-3'	
Col2a1	S	5'-ACCTTGGACGCCATGAAAGT-3'	Mouse
	AS	5'-CGGGAGGTCTTCTGTGATCG-3'	
Comp	S	5'-GTAAACACCGCCACTGATGA-3'	Mouse
	AS	5'-TGGGAGAAGCAGAAGACACC-3'	
Col9a2	S	5'-GATGGGTCCTCGTGGCTAT-3'	Mouse
	AS	5'-GTTCCCTTTGGGCCTGTTAT-3'	
Col6a3	S	5'-TTATGGTGCTGATGTTGACTGG-3'	Mouse
	AS	5'-ATTGCTGTTGGTTTGGTCGTT-3'	
Acan	S	5'-CCCAAGCACAGAGGTAAACAG-3'	Mouse
	AS	5'-CTCACATTGCTCCTGGTCTG-3'	
Dcn	S	5'-AGGCTTCCTACTCGGCTGTGA-3'	Mouse
	AS	5'-GTTCGGCGGCATTTGACTTT-3'	
Col6a1	S	5'-TGAAAATGTGCTCCTGCTGTG-3'	Mouse
	AS	5'-TGTCCCGTTGAGTGTCAGAA-3'	
Col9a1	S	5'-AGCTGATGGATTAACAGGACC-3'	Mouse
	AS	5'-TTCCCAGGGTCTCCAATAGG-3'	
Bgn	S	5'-GCATTGAGATGGGCGGGAA-3'	Mouse
	AS	5'-AGTAGGGCACAGGGTTGTTG-3'	
Chad	S	5'-ACAACCGCCTGAACCAACT-3'	Mouse
	AS	5'-GGGGAGGGATTCTGTGTCTT-3'	
Matn3	S	5'-CAGTGTGAGGGGTTTCTG-3'	Mouse
	AS	5'-AGCACCATAAGTTCATAGCG-3'	
HPRT1	S	5'-CCTGGCGTCGTGATTAGTG-3'	Human
	AS	5'-CTTGCGACCTTGACCATCTTT-3'	
TNKS1	S	5'-TCAGGGAACGATTTTGCTGGA-3'	Human
	AS	5'-ACTCTGGGTATGCCTGTTCTC-3'	
TNKS2	S	5'-GCGATACCCAAGGCAGACATT-3'	Human
	AS	5'-AACAAGAGGGCAGAGCAGATGG-3'	

Supplementary Table 2. List of PCR primers.

Genes	Strand	Primer sequences	Restriction Sites	Species
SOX9	S	5'-CCGAATTCATGAATCTCCTGGACCCCTTC-3'	EcoRI	Human
	AS	5'-CGTCTAGATCAAGGTCGAGTGAGCTGTGT -3'	XbaI	
TNKS2	S	5'-AAAAGCTTGGATCATGTCGGGTCGCCGCTG-3'	HindIII	Human
	AS	5'-AAGGATCCTTATCCATCGACCATACCTTCAGGCCTCATAA-3'	BamHI	

Supplementary Table 3. List of primers used for cloning.

Genes	Strand	Primer sequences	Deletion Sites	Species
SOX9	S	5'-CAGCCCCCTATCGACTTCCGCGA-3'	ΔTBD1	Human
	AS	5'-CCCCTCTCGCTTCAGGTCAGCCT-3'	772-792bp	
SOX9	S	5'-AGCAGCGACGTCATCTCCAACAT-3'	ΔTBD2	Human
	AS	5'-GAAGTCGATAGGGGGCTGTCT-3'	814-834bp	
SOX9	S	5'-AGCAGCGACGTCATCTCCAACAT-3'	ΔTBD1/2	Human
	AS	5'-CCCCTCTCGCTTCAGGTCAGCCT-3'	772-834bp	

Supplementary Table 4. List of primers used for mutagenesis.

Genes	Strand	Primer sequences	Species
Control	S	5'- CCGGAAACAAGATGAAGAGCACCAACTCGAGTTGGTGCTCTTCATCTTGTTTTTTTTG -3'	
	AS	5'- AATTCAAAAAAAACAAGATGAAGAGCACCAACTCGAGTTGGTGCTCTTCATCTTGTTT -3'	
TNKS1	S	5'-CCGGGCCCATAATGATGTCATGGAACTCGAGTTCCATGACATCATTATGGGCTTTTTG3'	Human
	AS	5'- AATTCAAAAAGCCCATAATGATGTCATGGAACTCGAGTTCCATGACATCATTATGGGC-3'	
TNKS2	S	5'- CCGGAAGGAAAGACGTAGTTGAATACTCGAGTATTCAACTACGTCTTTCCTTTTTTTG -3'	Human
	AS	5'- AATTCAAAAAAAGGAAAGACGTAGTTGAATACTCGAGTATTCAACTACGTCTTTCCTT -3'	
Tnks1	S	5'- CCGGGCTAGATGTGTTGGCTGATATCTCGAGATATCAGCCAACACATCTAGCTTTTTG-3'	Mouse
	AS	5'- AATTCAAAAAGCTAGATGTGTTGGCTGATATCTCGAGATATCAGCCAACACATCTAGG 3'	
Tnks2	S	5'- CCGGCATCGACACAAGCTGATTAAACTCGAGTTTAATCAGCTTGTGTCGATGTTTTTG -3'	Mouse
	AS	5'- AATTCAAAAACATCGACACAAGCTGATTAAACTCGAGTTTAATCAGCTTGTGTCGATG -3'	

Supplementary Table 5. List of primers used for shRNA plasmid construction.

Proteins involved in chondrogenesis (52 proteins)					
ALG2	CR3L2	GRN	NFKB2	Q9DAB5	SOX12
BMAL1	CREB1	GSK3A	NKX32	REL	SOX4
BMP2	CTNB1	GSK3B	PDGFA	RELB	SOX9
BMP4	CYR61	HHAT	PER1	RHOA	TF65
BMR1B	DHH	HIF1A	PP2BA	SHH	TNF12
CANB1	ENPP1	HMGB2	PP2BB	SIR1	VNN1
CANB2	FGF18	IHH	PP2BC	SMAD3	WNT3A
CBP	FGFR3	NFAC3	PRGC1	SOMA	
CHP1	GDF5	NFKB1	PTHR	SOX11	

Supplementary Table 6. List of mouse proteins in the IPA *chondrogenesis* category.

RESULTS

To screen for a key regulatory factor that could be targeted to initiate cartilage matrix anabolism, I conducted genetic analysis of transcriptomes of mouse reference populations using *post-hoc* factor analysis. First, I assessed transcriptional variance in the cartilage tissues of 16 strains of BXD mice (Suwanwela et al., 2011). I noted strong positive correlations among levels of transcripts encoding cartilage matrix genes (**Fig. 1a**) (Heinegard and Saxne, 2011). These high correlations were absent in organs without cartilaginous functions (**Fig. 1b**). I then attempted to extract a common axis underlying cartilage anabolism by performing a principal component analysis (PCA) on 14 highly inter-correlated cartilage matrix genes. The first axis I identified (Factor 1) essentially reflects the state of cartilage matrix anabolism (**Fig. 2a**). I further computed Pearson correlation coefficients between Factor 1 and various genes annotated as transcription factors, enzymes, or signaling molecules of unknown function in cartilage. Tankyrase (encoded by *Tnks1* or *Tnks2*) was found to possess a striking negative correlation with this anabolic axis as well as individual cartilage matrix genes*, Col2a1* and *Acan,* and was selected as a candidate (**Fig. 2a**,**b**).

a

Cartilage

b

Bone Femur   Kidney

Lung   Brain
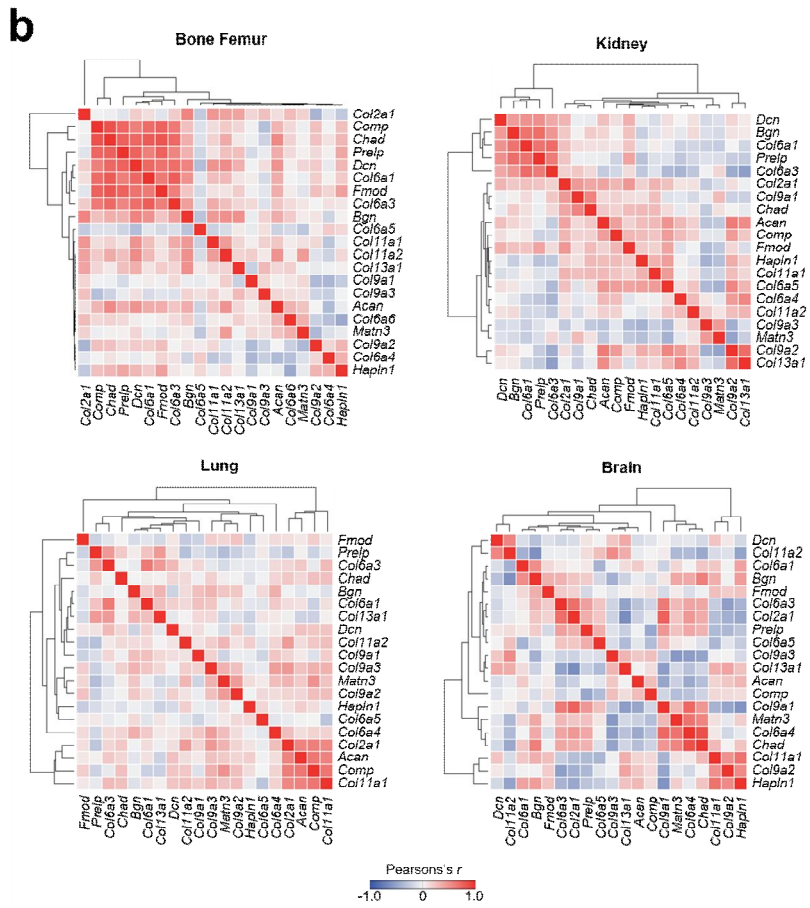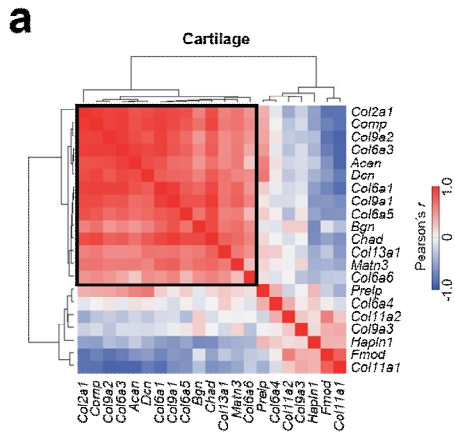
Pearsons's r
-1.0   0   1.0

Figure 1. There are positive inter-correlations among transcript levels of cartilage matrix genes in the cartilage tissues of 16 strains of BXD mice. (**a**) Heatmap of Pearson correlation coefficients of transcript levels for cartilage matrix genes in the cartilage tissue. (**b**) Heatmaps of Pearson correlation coefficients of transcript levels for cartilage matrix genes in bone femur, kidney, lung, and brain.
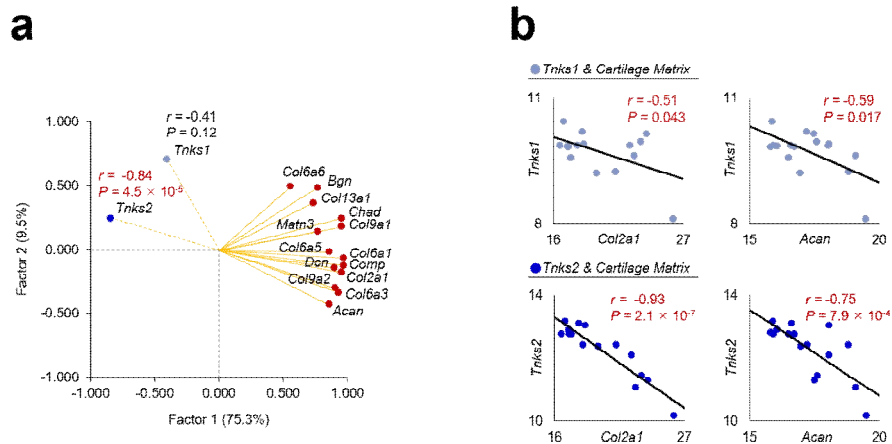
Figure 2. Identification of tankyrase as a candidate gene for cartilage anabolic genes regulator. (**a**) Factor loadings plot of 14 cartilage matrix genes in terms of transcript abundance, with *Tnks1/2* added to the plot. (**b**) Correlation between *Tnks1/2* and *Col2a1* or *Acan* mRNA levels.

Tankyrase belongs to the poly(ADP-ribose) polymerase (PARP) superfamily, which catalyzes addition of ADP-ribose moieties onto substrate proteins (Riffell et al., 2012; Levaot et al., 2011; Cho-Park and Steller, 2013; Guettler et al., 2011; Chang et al., 2005; Huang et al., 2009; Smith et al., 1998). Next, I examined the potential regulatory role of tankyrase in cartilage. Both tankyrase knockdown and specific inhibition by XAV939 (Huang et al., 2009) or IWR-1 (Huang et al., 2009) caused the collective expression of cartilage-specific matrix genes in chondrocytes (**Fig. 3a-c**). However, the PARP1/2 inhibitor ABT-888 failed to increase their expression (**Fig. 3c**).

Because mesenchymal progenitor cells are responsible for the regenerative capacity of damaged cartilage, I examined how tankyrase inhibition influences chondrogenic differentiation in mesenchymal stem cells[11,23]. Tankyrase inhibitors effectively induced chondrogenic nodule formation in micromass cultures of mouse limb-bud mesenchymal cells (**Fig. 4a**). Similarly, both pharmacological inhibition and knockdown of *TNKS1/2* effectively enhanced chondrogenic differentiation of human bone marrow–derived mesenchymal stem cells (hMSCs) (**Fig. 4b-d**). In contrast, tankyrase inhibition reduced osteogenesis and exerted no significant effect on adipogenesis of hMSCs (**Fig. 5a**,**b**).

I next evaluated the effect of tankyrase inhibition on stem cell–based restoration of hyaline cartilage. A full-thickness osteochondral lesion was filled with fibrin gel containing hMSCs transduced with control or *TNKS1/2* shRNAs. After 8 weeks, defects transplanted with hMSCs-control shRNA failed to fully recover hyaline cartilage organization, instead exhibiting features of fibrocartilage (**Fig. 6a-e**). However, lesions implanted with hMSCs-sh*TNKS1/2* had regenerated hyaline cartilage similar to articular cartilage, with robust accumulation of cartilage-specific matrix.
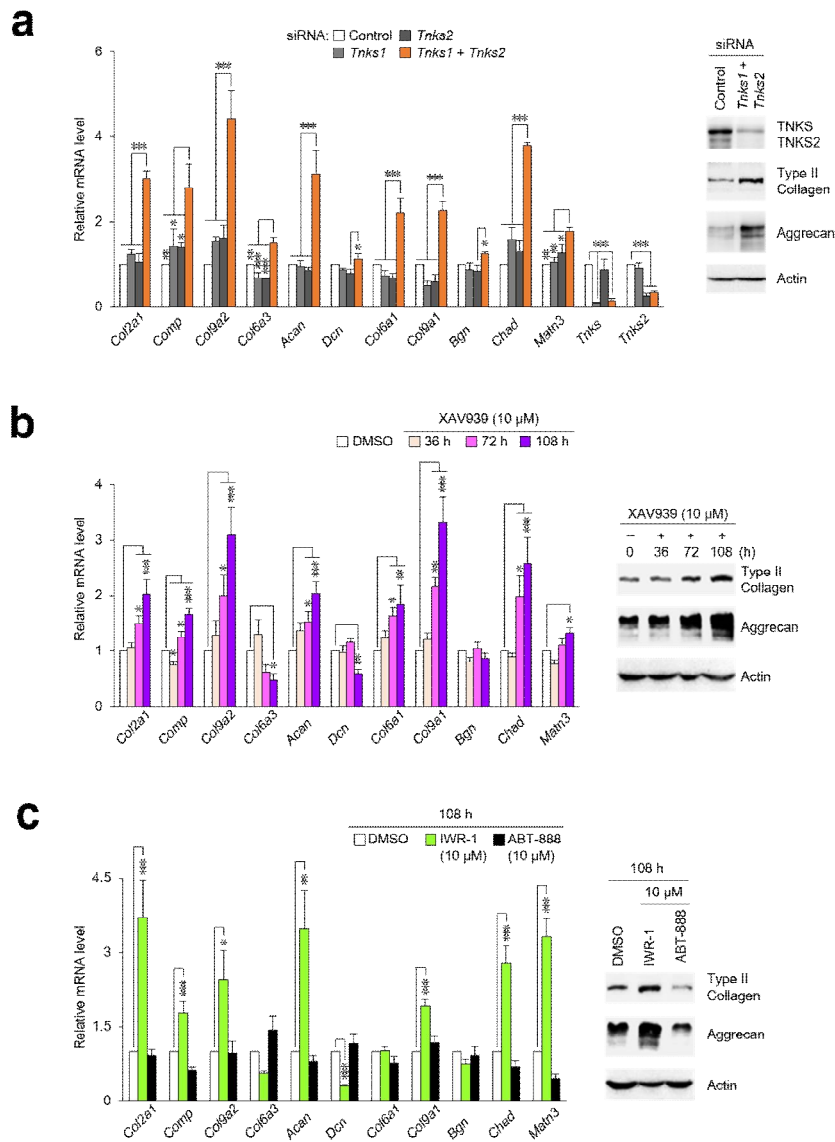
Figure 3. Tankyrase inhibition increases mRNA and protein levels of cartilage-specific matrix genes in mouse articular chondrocytes. (**a**) Mouse chondrocytes were treated with the indicated siRNAs ($n \geq 5$) or (**b,c**) drugs ($n = 7$). *Col6a5, Col6a6,* and *Col13a1* mRNAs were undetected. Data represent means ± s.e.m. *$P < 0.05$, **$P < 0.01$, ***$P < 0.001$; by *t* test (**a**) or ANOVA (**b,c**).

a

| DMSO | XAV939 | IWR-1 | ABT-888 |

Alcian Blue

Relative OD at 600nm (%)

b

Control shRNA | TNKS1/2 shRNA

Alcian Blue/Fast Red

c

shRNA: □ Control
■ TNKS1 + TNKS2

Relative mRNA level

TNKS1   TNKS2

d

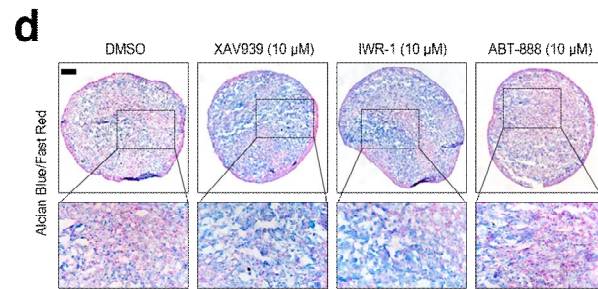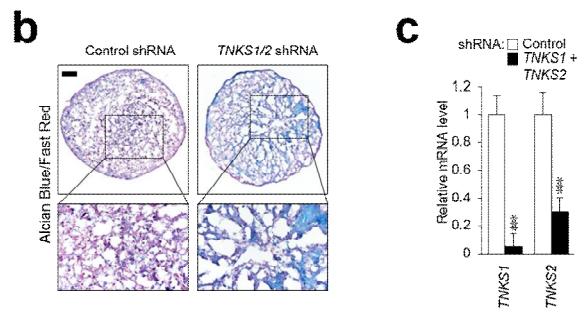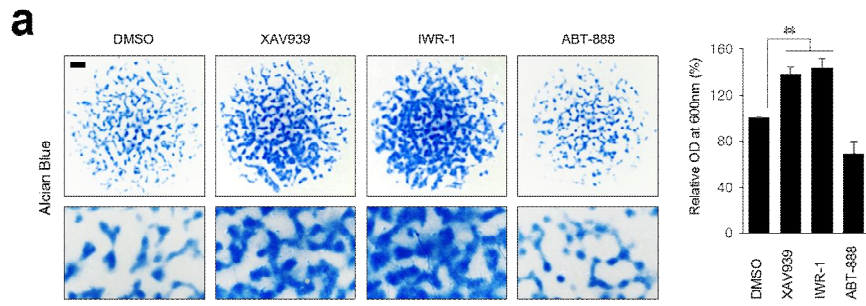| DMSO | XAV939 (10 μM) | IWR-1 (10 μM) | ABT-888 (10 μM) |

Alcian Blue/Fast Red

Figure 4. Tankyrase inhibition enhances chondrogenic differentiation in mesenchymal stem cells. (**a**) Alcian Blue staining of micromass cultured mouse limb-bud mesenchymal cells in the absence or presence of 10 μM of XAV939, IWR-1, or ABT-888 (left). Scale bar, 1 mm (top), 300 μm (bottom). Absorbance quantitation from stained cells (right; $n = 4$) (**b-d**) Histology of hMSC pellets stained by Alcian Blue. (b) Images of pellets infected with the indicated shRNA lentiviruses. (c) Knockdown efficiency of shRNAs ($n = 4$). (d) Images of pellets treated with the indicated drugs. Scale bars, 100 μm (**b,d**). Data represent means ± s.e.m. **$*P < 0.01$, ***$P < 0.001$; by ANOVA (**a**) or t test (**c**).
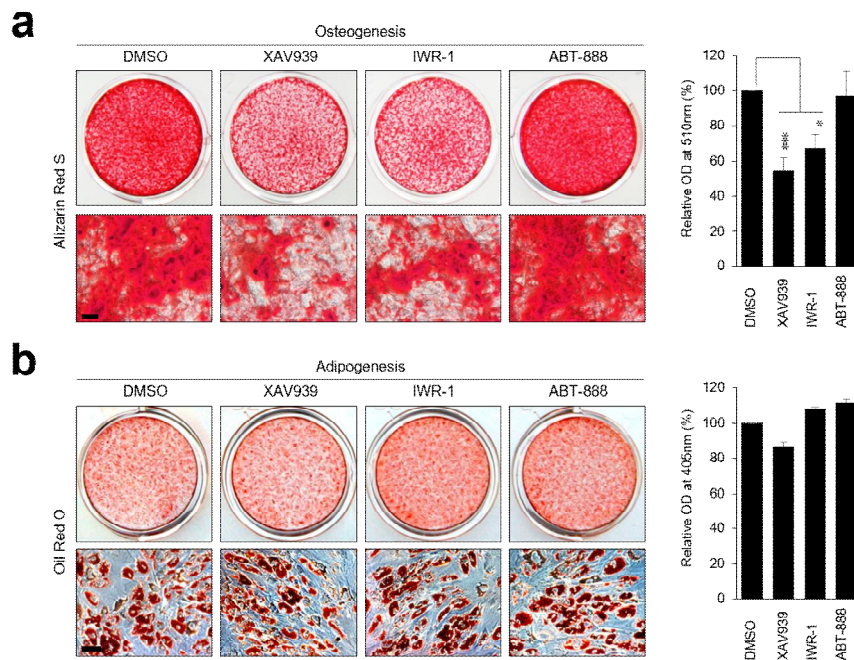
Figure 5. Tankyrase inhibition reduces osteogenesis and has no effect on adipogenesis. (**a**) Alizarin Red S Staining of osteogenesis-induced hMSCs in the absence or presence of 10 μM of XAV939, IWR-1, or ABT-888 (left). Scale bars, 100 μm. Absorbance of extracted Alizarin Red S from stained cells (right; $n \geq 6$). (**b**) Oil Red O staining of adipogenesis-induced hMSCs in the absence or presence of 10 μM of XAV939, IWR-1, or ABT-888 (left). Scale bars, 50 μm. Absorbance of extracted Oil Red O from stained cells (right; $n = 4$). Data represent means ± s.e.m. *$P < 0.05$, ***$P < 0.001$; by ANOVA (**a**,**b**).
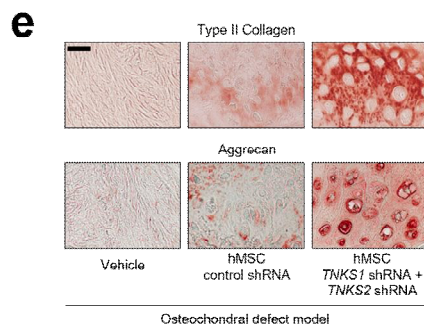
a

Fibrin only

Fibrin + hMSC-control shRNA

Fibrin + hMSC-*TNKS1/2* shRNA

b

Fibrin / Vehicle

Fibrin / hMSC control shRNA

Fibrin / hMSC *TNKS1* shRNA + *TNKS2* shRNA

Alcian Blue/Fast Red

c

ICRS macroscopic score (0-12)

☐ Fibrin only
■ Fibrin + hMSC

Vehicle

Control

TNKS1 + *TNKS2*

shRNA

d

☐ Fibrin only
▨ Fibrin + hMSC-control shRNA
■ Fibrin + hMSC-*TNKS1* shRNA + *TNKS2* shRNA

ICRS visual histological score (0-3)

Criteria: I. Surface   II. Matrix   III. Cell distribution   IV. Cell population viability   V. Subchondral bone

e

Type II Collagen

Aggrecan

Vehicle

hMSC control shRNA

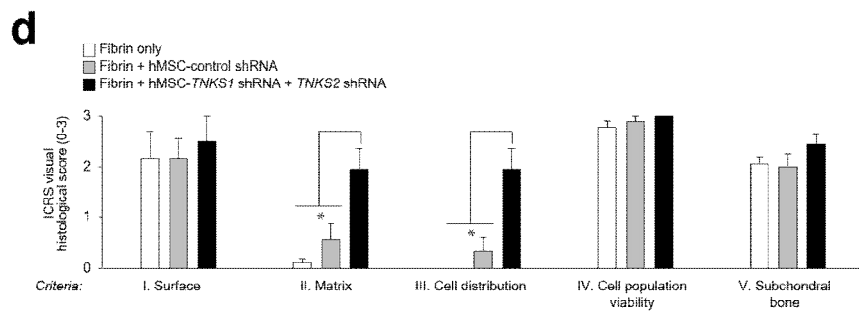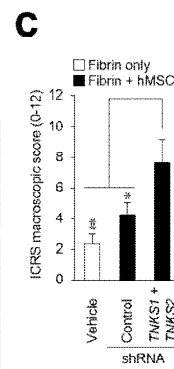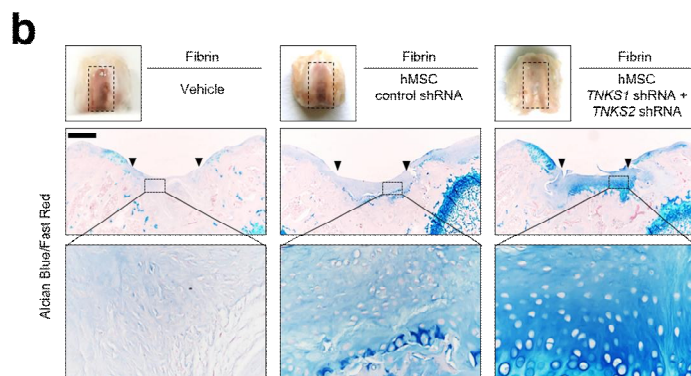hMSC *TNKS1* shRNA + *TNKS2* shRNA
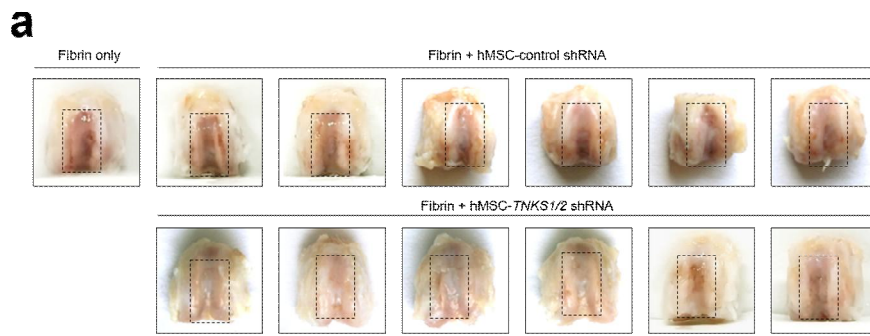
Osteochondral defect model

– 35 –

Figure 6. Knockdown of tankyrase in mesenchymal stem cells enhances *in vivo* cartilage repair in a rat osteochondral defect model. (**a**) hMSCs infected with control or *TNKS1/2* shRNA lentiviruses were implanted in the full-thickness cartilage lesions of rat knee joints with fibrin gel constructs. A fibrin-only group was used as a control. Gross appearance of the indicated groups 8 weeks after transplantation. Transplantation of hMSCs with *TNKS1/2* knockdown resulted in superior healing, filling lesions with cartilage-like tissues. (**b**) Gross appearance (top) and histological images (middle and bottom) of cartilage lesions. ▼ indicates the graft sites. (**c**) Cartilage regeneration as evaluated using the ICRS macroscopic score system ($n = 6$). (**d**) Cartilage repair was assessed using various criteria of the ICRS visual histological score system for *in vivo* repaired cartilage ($n = 6$) (**e**) immunostaining of cartilage matrix proteins, Type Ⅱ Collagen and Aggrecan. Data represent means ± s.e.m. *$P < 0.05$, **$P < 0.01$; by ANOVA.

Next, to elucidate the molecular mechanism of tankyrase function in regulating cartilage regeneration, I searched for tankyrase-interacting proteins by performing coimmunoprecipitation experiments followed by liquid chromatography-tandem mass spectrometry (LC-MS/MS) analysis (**Fig. 7a**,**b**). Candidate substrates were screened using a tankyrase- targeting score (TTS) system (**Fig. 7c**) (Guettler et al., 2011). Ingenuity pathway analysis (IPA) revealed that 4 candidate proteins above the TTS cutoff fell into the *chondrogenesis* category. Unlikely targets, with tankyrase-binding motifs in a structured region, were further filtered out by IUPred disorder score (**Fig. 7d**) (Dosztanyi et al., 2005). SOX9 showed high TTS and disorder scores.

Binding of tankyrase with SOX9 was confirmed by immunoprecipitation assays (**Fig. 7e** and **Fig. 8a**). Moreover, interaction between Tankyrase and SOX9 was shown in mouse chondrocytes by a Duolink assay (**Fig. 8b**). The two tankyrase-binding domains (TBDs) of SOX9, designated TBD1 and TBD2, are highly conserved among vertebrates (**Fig. 9a**). Based on structural simulations, the TBD1 and TBD2 peptides fit into the binding pocket located central to the ankyrin repeat cluster (ARC) domains of tankyrase, in which known substrates, 3BP2 and MCL1, are aligned (**Fig. 9b**). Indeed, deletion of either TBD1 or TBD2 significantly impaired the binding affinity of SOX9 for tankyrase (**Fig. 9c**); simultaneous deletion of both TBDs nearly abolished the association (**Fig. 9d**). Consistently, wild-type SOX9 underwent extensive poly(ADP-ribosyl)ation (PARylation), whereas the SOX9 mutant missing both TBDs exhibited a markedly reduced extent of PARylation (**Fig. 9e**).

SOX9, a master transcription factor of chondrogenesis, transcribes various cartilage-specific matrix genes (Ohba et al., 2015). I explored whether tankyrase inhibition affected the transcriptional activity of SOX9. Tankyrase inhibition using various classes of drugs or siRNAs specifically increased the transcriptional activity of SOX9 (**Fig. 10a-c**).
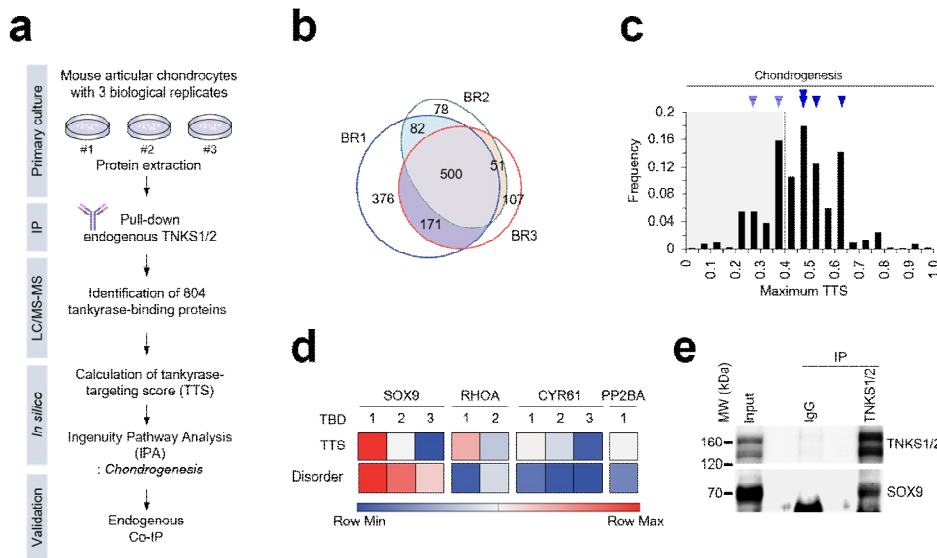
Figure 7. Identification of SOX9 as a novel tankyrase substrate. (**a**) Flowchart of tankyrase substrate identification in chondrocytes. (**b**) Venn diagram illustrating the overlap of tankyrase-binding proteins identified by three biological replicates (BR) using LC/MS-MS. (**c**) Histogram of the maximum TTS of the identified tankyrase-binding proteins. ▼ indicate the bins that include proteins implicated in chondrogenesis. (**d**) Heatmap of the TTS and disorder score of TBDs from the predicted tankyrase-binding proteins. (**e**) Coimmunoprecipitation of endogenous TNKS1/2 with SOX9 in chondrocytes.
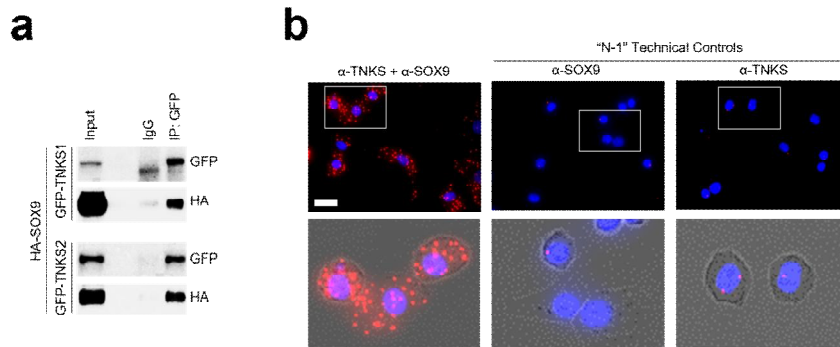
Figure 8. Endogenous interaction between tankyrase and SOX9. (**a**) Pull-down assays of GFP-tagged TNKS or TNKS2 with HA-tagged SOX9 in HEK293T cells. (**b**) Detection of TNKS1/2 and SOX9 co-localization (red) in mouse chondrocytes by a Duolink assay. DAPI staining (blue). Scale bars, 25 μm (top) and 10μm (bottom).
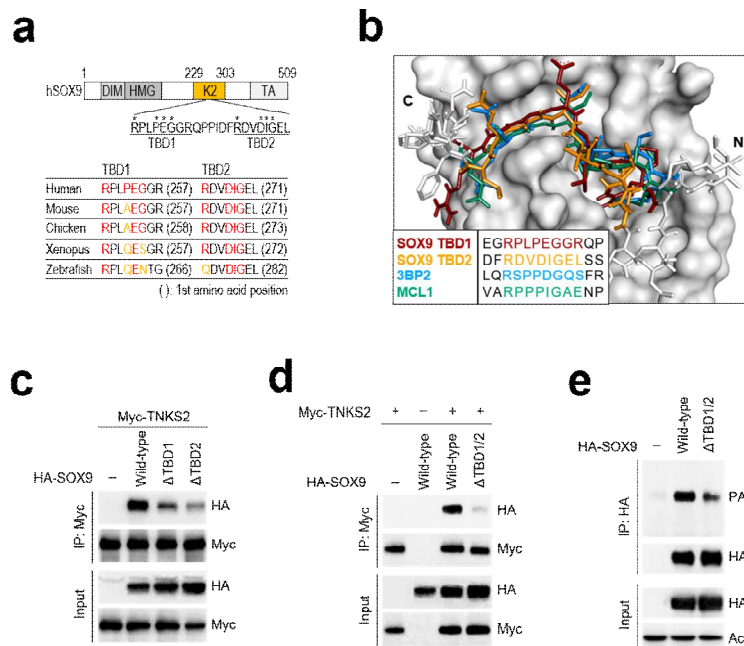
Figure 9. Tankyrase binding domain 1 and 2 of SOX9 are responsible for tankyrase binding. (**a**) Schematic representation of the predicted TBDs in human SOX9 protein (top) and sequence alignment of TBD1 and TBD2 of SOX9 among vertebrates (bottom). Colored letters indicate the consensus amino acid sequence of TBDs. (**b**) Superimposition of TNKS2:3BP2 and TNKS2:MCL1 complexes with TNKS2 bound to SOX9-TBD1/2. (**c**) Pull-down assays of Myc-tagged TNKS2 with HA-tagged wild-type SOX9 or TBD1 or TBD2 deleted SOX9 mutants in HEK293T cells. (**d**) Pull-down assay of TNKS2 with wild-type or TBD1/2-deleted SOX9 in HEK293T cells. (**e**) PARylation of wild-type or TBD1/2-deleted SOX9 in HEK293T cells.
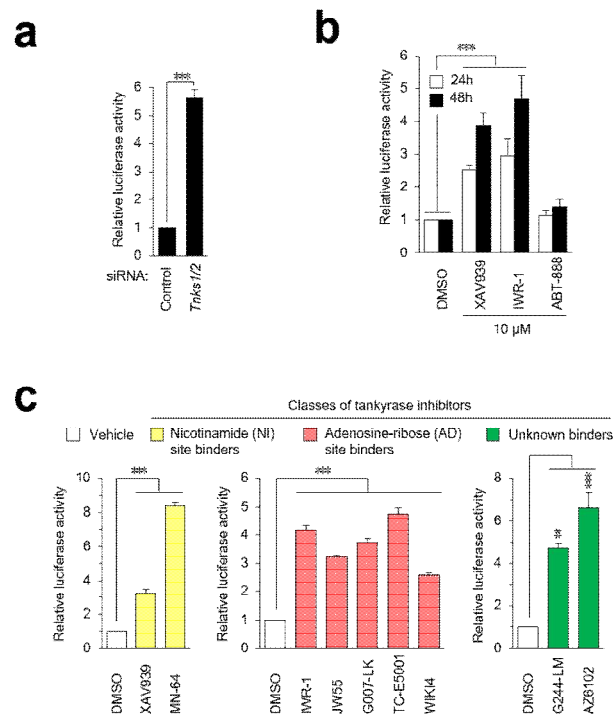
Figure 10. Tankyrase inhibition enhances the transcriptional activity of SOX9. (**a-c**) SOX9-dependent *Col2a1* enhancer activity was measured with a reporter gene assay in mouse articular chondrocytes after (**a**) siRNA (*n* = 3) or (**b**) drugs (*n* ≥ 5). (**c**) SOX9 reporter gene assay in mouse articular chondrocytes treated with 10 μM of various classes of tankyrase inhibitors for 48 h (*n* = 3). Data represent means ± s.e.m. **P < 0.01, ***P < 0.001; by *t* test (**a**) or ANOVA (**b**,**c**).

Based on its overall pro-regenerative effects at the cellular level, I evaluated the efficacy of tankyrase inhibition in treating OA cartilage *in vivo,* using surgical destabilization of the medial meniscus (DMM) in mice (**Fig. 12** and **Fig. 13**). For stable and prolonged delivery of tankyrase inhibitors to mouse knee joints, I used injectable hydrogels made of ascorbyl palmitate (Zhang et al., 2015). Intra-articular (IA) injection of this hydrogel-based drug delivery system allowed controlled release of the loaded small molecule to the articular cartilage over 9 days (**Fig. 11a,b**). IA administration of XAV939 or IWR-1 significantly reduced surgically induced OA cartilage destruction 8 weeks after surgery (**Fig. 12a-c**). A concomitant increase in type II collagen and aggrecan was observed, further supporting the pro-anabolic effects of tankyrase inhibition *in vivo* (**Fig. 12d**).

I further tested the potential of tankyrase inhibition to repair mid-to-late stage OA defects. Using a DMM model in mice, I previously showed that early osteoarthritic lesions are observed 2 weeks after surgery (Kim et al., 2015), and the disease progresses to the mid-to-late stage 6 weeks after surgery (**Fig. 13b**, left). Following drug exposure for an additional 6 weeks (**Fig. 13a**), vehicle-treated mice experienced further OA progression and damage of cartilage (**Fig. 13b**, center). In contrast, XAV939 treatment to mid-to-late stage OA mice attenuates articular cartilage destruction (**Fig. 13b**, right). Taken together, my results clearly indicate that tankyrase inhibition exerts regenerative effects in mice, highlighting its promise as a therapeutic strategy for OA.
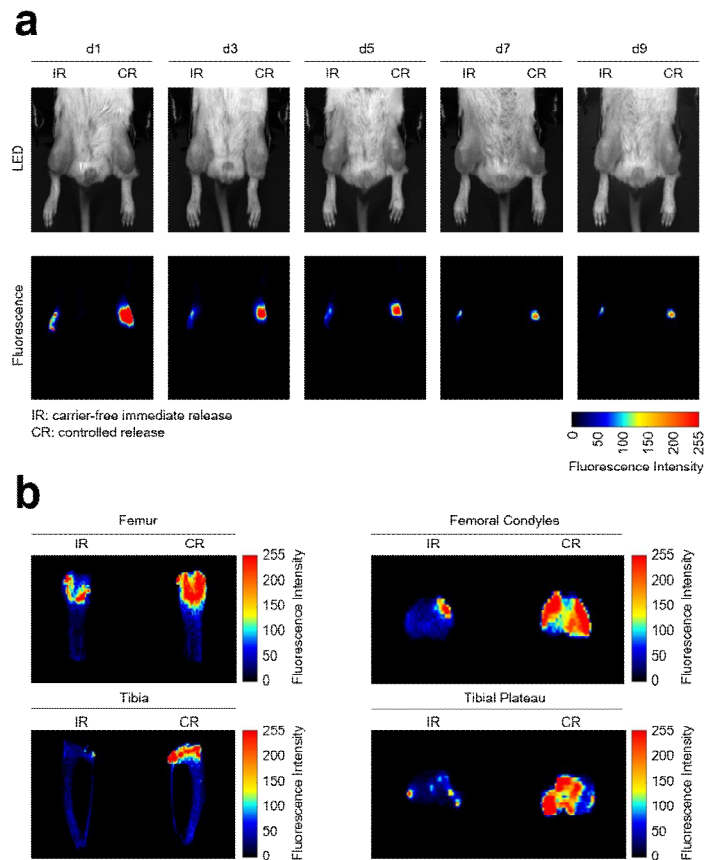
Figure 11. Hydrogel made from ascorbyl palmitate mediates controlled release in mouse knee joints. (**a**) Light-emitting diode (LED) and fluorescence images of mouse knee joints intra-articularly injected with carrier-free DiD or DiD-loaded ascorbyl palmitate hydrogel. Images were acquired on the indicated days after injection. (**b**) Fluorescence images of mouse femur (femoral condyle) and tibia (tibial plateau) with carrier-free DiD or DiD-loaded ascorbyl palmitate hydrogel. Images were acquired at 9 days after IA injection.
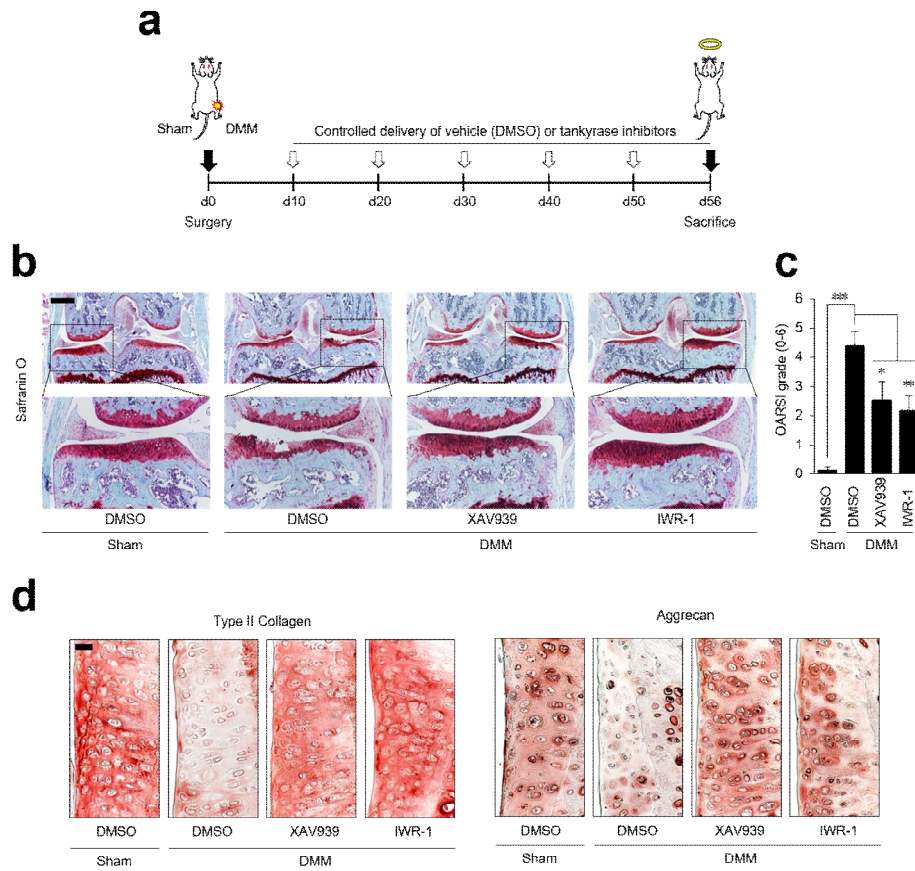
Figure 12. Tankyrase inhibition enhances cartilage repair in a surgically-induced OA model. (**a**) Schematic illustration of the destabilization of the medial meniscus (DMM) model and treatment schedule in mouse. (**b,c**) Cartilage destruction assessed by (**b**) Safranin O staining and (**c**) OARSI grade (*n* = 10). (**d**) Immunohistochemical staining for cartilage matrix proteins, Type Ⅱ Collagen and Aggrecan. Data represent means ± s.e.m. *P < 0.05, **P < 0.01, ***P < 0.001; by Mann-Whitney *U* test.
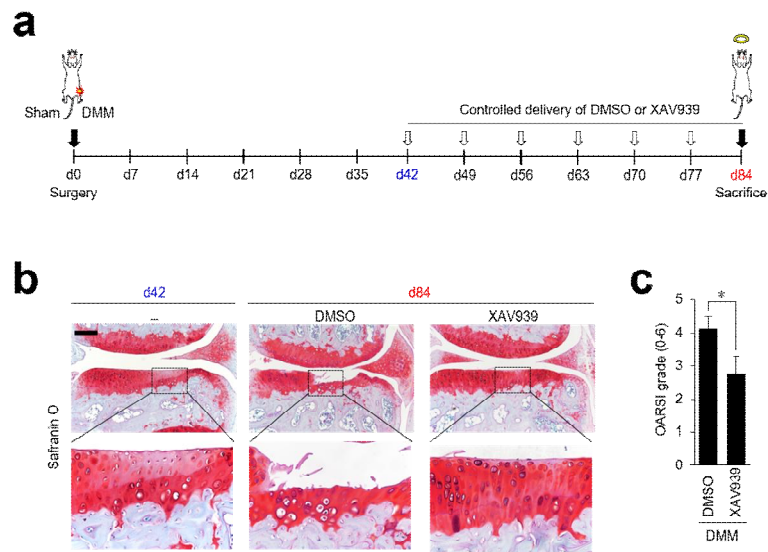
Figure 13. Tankyrase inhibitor XAV939 enhances cartilage repair in advanced OA. (**a**) Schematic representation of controlled drug delivery to DMM-operated mice. (**b**) Cartilage destruction assessed by Safranin O staining ($n \geq 14$). Scale bar: 200 μm. (**c**) OARSI grades of articular Cartilage destruction for the vehicle- (n = 14) and XAV939-treated groups (n = 15). Data represent means ± s.e.m. *$P < 0.05$; by Mann-Whitney *U* test.

DISCUSSION

OA is degenerative disease, which involves progressive and irreversible destruction of articular cartilage. In this perspective, previous studies have focused on the discovery of several key catabolic regulators contributing to cartilage destruction (Liu-Bryan and Terkeltaub, 2015; Kim et al., 2014).

I analyzed cartilage matrix anabolism in mouse cartilage to find a regulator of it. This trial has not been approached in previous studies and can be a effective strategy for repairing cartilage. Identifying and controlling the regulator of cartilage matrix genes suggests potent way to activate the innate repair system blocked in degenerative cartilage tissue of mammals.

The target of tankyrase in chondrocytes that I newly identified is SOX9. Surprisingly, SOX9 is a master transcription factor of inducing cartilage-specific matrix genes and chondrogenesis (Ohba et al., 2015). In a recent report, SOX9 expression was upregulated at stage 1 and suppressed at a later stage of OA progression (Zhang et al., 2015). This means that early OA is associated with increased anabolic gene expression as a reaction to recovery damages and SOX9 plays a key role in repair cartilage. However, at a later stage of OA, SOX9 activity is not maintained and insufficient to counter the increase in catabolic matrix degrading enzymes. Therefore, upregulation of SOX9 activity through tankyrase inhibition may enhance power to repair cartilage. Chondrocytes and chondrogenic progenitor cells obtain more chondrogenic features and express many ECM genes.

Tankyrase is well known for its role in regulating Wnt/β-Catenin Signaling pathway (Huang et al., 2009). Axin is a component of the β-catenin destruction complex and tankyrase PARylates Axin. RNF146, a RING-domain E3 ubiquitin ligase promotes degradation of PARsylated Axin

by ubiquitylation (Zhang et al., 2011). Thus, it was thought that the effect of tankyrase inhibition is a result of RNF146-Axin-dependent regulation. However, in my study, the broad regulation of anabolic catilage matrix genes by tankyrase inhibition is not explained only through Wnt/β-Catenin Signaling. SOX9, newly identified target of tankyrase, may explain the pro-regeneration in cartilage.

In further study to verify this accurately, it will be required to test that the regulation of RNF146 or axin also has an anabolic effect of Tankyrase inhibition in chondrocytes. RNF146-independent effects of tankyrase inhibition may propose a completely novel mechanism in tankyrase-mediated mechanisms.

Overall, tankyrase inhibition is not only a wnt inhibition effect that limits catabolic degradation pathway, but also direct activation of SOX9 boosting innate repair capacity (**Fig. 14**). In particular, I raise the intriguing possibility that tankyrase inhibition elicits regenerative signals for reconstruction of cartilage at both the molecular and organismal levels. I expect my findings to provide guidelines for future development of OA therapies aimed at functional repair of articular cartilage.

Finally, my findings have direct implications for developing therapeutic strategies for OA by stimulating innate regeneration of cartilage. The regenerative capacity of tankyrase inhibition may be attributable to combinatorial effects, promoting the expression of cartilage-specific matrix proteins by chondrocytes and stimulating the chondrogenesis of stem cells in the joint. I expect my findings to provide guidelines for future development of OA therapies aimed at functional repair of articular cartilage.
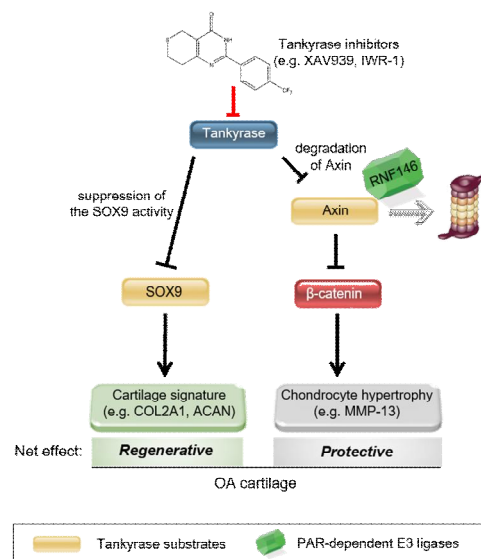
Figure 14. Schematic representation of the molecular mechanisms underlying the therapeutic effects of tankyrase inhibitors in OA. Chemical structure of XAV939 was drawn by ChemDraw.

REFERENCES

Alberts, R., Lu, L., Williams, R. W., & Schughart, K. (2011). Genome-wide analysis of the mouse lung transcriptome reveals novel molecular gene interaction networks and cell-specific expression signatures. *Respiratory research*, *12*(1), 61.

Blom, A. B., van Lent, P. L., Libregts, S., Holthuysen, A. E., van der Kraan, P. M., van Rooijen, N., & van den Berg, W. B. (2007). Crucial role of macrophages in matrix metalloproteinase–mediated cartilage destruction during experimental osteoarthritis: involvement of matrix metalloproteinase 3. *Arthritis & Rheumatology*, *56*(1), 147-157.

Chambers, M. C., Maclean, B., Burke, R., Amodei, D., Ruderman, D. L., Neumann, S., ... & Hoff, K. (2012). A cross-platform toolkit for mass spectrometry and proteomics. *Nature biotechnology*, *30*(10), 918-920.

Chang, P., Coughlin, M., & Mitchison, T. J. (2005). Tankyrase-1 polymerization of poly (ADP-ribose) is required for spindle structure and function. *Nature cell biology*, *7*(11), 1133-1139.

Cho-Park, P. F., & Steller, H. (2013). Proteasome regulation by ADP-ribosylation. *Cell*, *153*(3), 614-627.

Diekman, B. O., & Guilak, F. (2013). Stem cell-based therapies for osteoarthritis: challenges and opportunities. *Current opinion in rheumatology*, 25(1), 119.

Dosztányi, Z., Csizmok, V., Tompa, P., & Simon, I. (2005). IUPred: web server for the prediction of intrinsically unstructured regions of proteins based on estimated energy content. *Bioinformatics*, *21*(16), 3433-3434.

Embree, M. C., Chen, M., Pylawka, S., Kong, D., Iwaoka, G. M., Kalajzic, I., ... & Koslovsky, D. A. (2016). Exploiting endogenous fibrocartilage stem cells to regenerate cartilage and repair joint injury. *Nature communications*, *7*, 13073.

Farber, C. R., van Nas, A., Ghazalpour, A., Aten, J. E., Doss, S., Sos, B., ... & Smith, D. J. (2009). An integrative genetics approach to identify candidate genes regulating BMD: combining linkage, gene expression, and association. *Journal of Bone and Mineral Research*, *24*(1), 105-116.

Farr, J. N., Xu, M., Weivoda, M. M., Monroe, D. G., Fraser, D. G., Onken, J. L., ... & LeBrasseur, N. K. (2017). Targeting cellular senescence prevents age-related bone loss in mice. *Nature Medicine*, *23*(9), 1072-1079.

Glasson, S. S., Askew, R., Sheppard, B., Carito, B., Blanchet, T., Ma, H. L., ... & Majumdar, M. K. (2005). Deletion of active ADAMTS5 prevents cartilage degradation in a murine model of osteoarthritis. *Nature*, *434*(7033), 644-648.

Glasson, S. S., Blanchet, T. J., & Morris, E. A. (2007). The surgical destabilization of the medial meniscus (DMM) model of osteoarthritis in the 129/SvEv mouse. *Osteoarthritis and Cartilage*, *15*(9), 1061-1069.

Glasson, S. S., Chambers, M. G., Van Den Berg, W. B., & Little, C. B. (2010). The OARSI histopathology initiative–recommendations for histological

assessments of osteoarthritis in the mouse. *Osteoarthritis and cartilage*, *18*, S17-S23.

Gosset, M., Berenbaum, F., Thirion, S., & Jacques, C. (2008). Primary culture and phenotyping of murine chondrocytes. *Nature protocols*, *3*(8), 1253-1260.

Guettler, S., LaRose, J., Petsalaki, E., Gish, G., Scotter, A., Pawson, T., ... & Sicheri, F. (2011). Structural basis and sequence rules for substrate recognition by Tankyrase explain the basis for cherubism disease. *Cell*, *147*(6), 1340-1354.

Haikarainen, T., Krauss, S., & Lehtio, L. (2014). Tankyrases: structure, function and therapeutic implications in cancer. *Current pharmaceutical design*, *20*(41), 6472-6488.

Heinegård, D., & Saxne, T. (2011). The role of the cartilage matrix in osteoarthritis. *Nature Reviews Rheumatology*, *7*(1), 50-56.

Heinemeier, K. M., Schjerling, P., Heinemeier, J., Møller, M. B., Krogsgaard, M. R., Grum-Schwensen, T., ... & Kjaer, M. (2016). Radiocarbon dating reveals minimal collagen turnover in both healthy and osteoarthritic human cartilage. *Science translational medicine*, 8(346), 346ra90-346ra90.

Huang, S. M. A., Mishina, Y. M., Liu, S., Cheung, A., Stegmeier, F., Michaud, G. A., ... & Hild, M. (2009). Tankyrase inhibition stabilizes axin and antagonizes Wnt signalling. *Nature*, *461*(7264), 614-620.

Jeon, O. H., Kim, C., Laberge, R. M., Demaria, M., Rathod, S., Vasserot, A. P., ... & Baker, D. J. (2017). Local clearance of senescent cells attenuates the development of post-traumatic osteoarthritis and creates a pro-regenerative environment. *Nature Medicine*, *23*(6), 775-781.

Johnson, K., Zhu, S., Tremblay, M. S., Payette, J. N., Wang, J., Bouchez, L. C., ... & Schultz, P. G. (2012). A stem cell–based approach to cartilage repair. *Science*, 336(6082), 717-721.

Kilkenny, C., Browne, W. J., Cuthill, I. C., Emerson, M., & Altman, D. G. (2010). Improving bioscience research reporting: the ARRIVE guidelines for reporting animal research. *PLoS biology*, *8*(6), e1000412.

Kim, J. H., Jeon, J., Shin, M., Won, Y., Lee, M., Kwak, J. S., ... & Chun, J. S. (2014). Regulation of the catabolic cascade in osteoarthritis by the zinc-ZIP8-MTF1 axis. *Cell*, *156*(4), 730-743.

Kim, J. H., Lee, G., Won, Y., Lee, M., Kwak, J. S., Chun, C. H., & Chun, J. S. (2015). Matrix cross-linking–mediated mechanotransduction promotes posttraumatic osteoarthritis. *Proceedings of the National Academy of Sciences*, *112*(30), 9424-9429.

Kim, J. S., Monroe, M. E., Camp, D. G., Smith, R. D., & Qian, W. J. (2013). In-source fragmentation and the sources of partially tryptic peptides in shotgun proteomics. *Journal of proteome research*, *12*(2), 910-916.

Kim, S., & Pevzner, P. A. (2014). MS-GF makes progress towards a universal database search tool for proteomics. Nat Commun 5: 5277.

Lee, H., Heo, L., Lee, M. S., & Seok, C. (2015). GalaxyPepDock: a protein–peptide docking tool based on interaction similarity and energy optimization. *Nucleic acids research*, *43*(W1), W431-W435.

Lehtiö, L., Chi, N. W., & Krauss, S. (2013). Tankyrases as drug targets. *The FEBS journal*, *280*(15), 3576-3593.

Levaot, N., Voytyuk, O., Dimitriou, I., Sircoulomb, F., Chandrakumar, A., Deckert, M., ... & Cong, F. (2011). Loss of Tankyrase-mediated destruction of 3BP2 is the underlying pathogenic mechanism of cherubism. *Cell*, *147*(6), 1324-1339.

Little, C. B., Barai, A., Burkhardt, D., Smith, S. M., Fosang, A. J., Werb, Z., ... & Thompson, E. W. (2009). Matrix metalloproteinase 13–deficient mice are resistant to osteoarthritic cartilage erosion but not chondrocyte hypertrophy or osteophyte development. *Arthritis & Rheumatology*, *60*(12), 3723-3733.

Liu-Bryan, R., & Terkeltaub, R. (2015). Emerging regulators of the inflammatory process in osteoarthritis. *Nature Reviews Rheumatology*, *11*(1), 35-44.

Mainil-Varlet, P., Aigner, T., Brittberg, M., Bullough, P., Hollander, A., Hunziker, E., ... & Stauffer, E. (2003). Histological assessment of cartilage repair: a report by the Histology Endpoint Committee of the International Cartilage Repair Society (ICRS). *JBJS*, *85*(suppl_2), 45-57.

Micallef, L., & Rodgers, P. (2014). eulerAPE: drawing area-proportional 3-Venn diagrams using ellipses. *PloS one*, *9*(7), e101717.

Murakami, S., Lefebvre, V., & De Crombrugghe, B. (2000). Potent Inhibition of the Master Chondrogenic FactorSox9 Gene by Interleukin-1 and Tumor Necrosis Factor-α. *Journal of Biological Chemistry*, *275*(5), 3687-3692.

Ohba, S., He, X., Hojo, H., & McMahon, A. P. (2015). Distinct transcriptional programs underlie Sox9 regulation of the mammalian chondrocyte. *Cell reports*, *12*(2), 229-243.

Perez-Llamas, C., & Lopez-Bigas, N. (2011). Gitools: analysis and visualisation of genomic data using interactive heat-maps. *PloS one*, *6*(5), e19541.

Riffell, J. L., Lord, C. J., & Ashworth, A. (2012). Tankyrase-targeted therapeutics: expanding opportunities in the PARP family. *Nature reviews Drug discovery*, *11*(12), 923-936.

Saba, L., Bhave, S. V., Grahame, N., Bice, P., Lapadat, R., Belknap, J., ... & Tabakoff, B. (2006). Candidate genes and their regulatory elements: alcohol preference and tolerance. *Mammalian Genome*, *17*(6), 669-688.

Sakata, K., Furumatsu, T., Abe, N., Miyazawa, S., Sakoma, Y., & Ozaki, T. (2013). Histological analysis of failed cartilage repair after marrow stimulation for the treatment of large cartilage defect in medial compartmental osteoarthritis of the knee. *Acta Medica Okayama*, 67(1), 65-74.

Smith, S., Giriat, I., Schmitt, A., & De Lange, T. (1998). Tankyrase, a poly (ADP-ribose) polymerase at human telomeres. *Science*, *282*(5393), 1484-1487.

Suwanwela, J., Farber, C. R., Haung, B. L., Song, B., Pan, C., Lyons, K. M., & Lusis, A. J. (2011). Systems genetics analysis of mouse chondrocyte differentiation. *Journal of Bone and Mineral Research*, *26*(4), 747-760.

Van Den Borne, M. P. J., Raijmakers, N. J. H., Vanlauwe, J., Victor, J., de Jong, S. N., Bellemans, J., & Saris, D. B. F. (2007). International Cartilage Repair Society (ICRS) and Oswestry macroscopic cartilage evaluation scores validated for use in Autologous Chondrocyte Implantation (ACI) and microfracture. *Osteoarthritis and cartilage*, *15*(12), 1397-1402.

Wieland, H. A., Michaelis, M., Kirschbaum, B. J., & Rudolphi, K. A. (2005). Osteoarthritis—an untreatable disease?. *Nature reviews Drug discovery*, 4(4), 331-344.

Zhang, Q., Ji, Q., Wang, X., Kang, L., Fu, Y., Yin, Y., ... & Wang, Y. (2015). SOX9 is a regulator of ADAMTSs-induced cartilage degeneration at the early stage of human osteoarthritis. *Osteoarthritis and cartilage*, *23*(12), 2259-2268.

Zhang, S., Ermann, J., Succi, M. D., Zhou, A., Hamilton, M. J., Cao, B., ... & Traverso, G. (2015). An inflammation-targeting hydrogel for local drug delivery in inflammatory bowel disease. *Science translational medicine*, *7*(300), 300ra128-300ra128.

Zhang, Y., Liu, S., Mickanin, C., Feng, Y., Charlat, O., Michaud, G. A., ... & Myer, V. E. (2011). RNF146 is a poly (ADP-ribose)-directed E3 ligase that regulates axin degradation and Wnt signalling. *Nature cell biology*, *13*(5).

국문초록

탄키라아제 억제를 통한 골관절염 연골의 내재된 회복 능력 활성화

김수경

자연과학대학 생명과학부

서울대학교 대학원

골관절염(osteoarthritis)은 만성 퇴행성 질환으로 관절 연골의 점진적이고 비가역적인 파괴를 수반하는 질환이다. 골관절염 환자의 연골을 재생시키려는 노력에도 불구하고, 성인 연골이 지닌 재생 능력의 한계로 골관절염의 완전한 치료는 어렵다. 나는 이 연구에서 연골재생을 유도할 수 있는 인자를 찾아 새로운 골관절염 치료 전략을 제시하고자 한다. 나는 우선 마우스 레퍼런스 집단에서 시스템 수준 요인 분석(factor anaylsis)을 통해 연골형성 유전자들의 발현을 조절하는 인자로 탄키라아제(tankyrase)를 발굴했다. 탄키라아제 억제는 마우스 연골세포에서 연골 특이적 세포 외 기질(extracellular matrix) 유전자의 발현을 증가시킨다. 또한, 탄키라아제 억제는 중간엽 줄기세포의 연골세포로의 분화를 촉진한다. 랫트(rat)의 골연골 병변(osteochondral defect) 모델에서는 탄키라아제를 억제한 중간엽 줄기세포를 주입시 연골 병변이 재생됨을 확인했다. 탄키라아제 억제는 연골세포의 마스터 전사인자(master transcription factor)인 SOX9의 전사인자 활성 조절을 통해 연골재생을 유도한다. 나는 탄키라아제가 SOX9에 결합해 SOX9을

poly(ADP-ribosyl)ation화시킴을 확인했다. 더불어, 골관절염이 유도된 마우스(mouse) 모델에 하이드로젤 기반으로 탄키라아제 억제제를 전달해 골관절염의 진행을 억제했다. 위의 결과들은 탄키라아제 저해를 통한 새로운 골관절염 치료 전략을 제시한다.

······································

주요어 : 탄키라아제(tankyrase), 골관절염(osteoarthritis),
          연골재생(cartilage repair), SOX9, PARylation
학 번 : 2016-20376